Plasma Sources Sci. Technol. **9** (2000) 1–9. Printed in the UK PII: S0963-0252(00)12137-1

The influence of antenna configuration and standing wave effects on density profile in a large-area inductive plasma source

Yaoxi Wu† and M A Lieberman‡

† Department of Materials Science and Engineering, University of California, Berkeley, CA 94720, USA
‡ Department of Electrical Engineering and Computer Sciences, University of California, Berkeley, CA 94720, USA

Sunrise Setting
Marked Proof
PSST/112137/PAP
19026e
Printed on 9/3/00
at 15.43

Received 14 September 1999, in final form 16 February 2000

Abstract. The electrical and plasma properties of a large-area inductive plasma source are investigated. The source is a 71 cm × 61 cm × 20 cm metal chamber providing a processing area of 37 cm × 47 cm for large-size wafers and glass substrates for flat panel displays. The exciting antenna is embedded inside the processing chamber, and the rf power is inductively coupled from the antenna to the plasma through thin (1.7 mm thick) quartz tubes. A tuning network is used to launch a travelling wave or a wave with a desired standing-wave ratio. The antenna–plasma system is modelled as a lossy transmission line, and a transformer model is applied to study the electrical properties of the system. The model is used to evaluate the conditions required to launch a travelling wave, and these conditions are verified experimentally. The plasma density distributions under various operating conditions are measured with Langmuir probes and compared to a global model for inductive discharges. Our experiments show that high plasma densities are produced over a large area, and that the density profiles are strongly influenced by the antenna configuration and standing-wave effects.

1. Introduction

Inductively coupled plasma sources have been studied extensively by many researchers in the past ten years. The driving forces for the effort are the recognition of their capability to generate a high density under low pressure and the independent control of ion flux and ion-bombarding energy. The former is desirable to increase the processing speed, and the latter is favourable for minimizing the contamination, substrate damage, and power loss due to the ion bombardment of the chamber walls and substrates. A common feature of these high-density sources is that the rf power is coupled to the plasma across a dielectric medium, rather than by direct connection to an electrode in the plasma as in a capacitively coupled plasma source. This non-capacitive power transfer is the key to achieving low voltages across all plasma sheaths at electrode and wall surfaces, obtaining a high-plasma density. Although inductively coupled sources have many merits, the plasmas are inherently non-uniform, especially when the exciting antenna is scaled to a size comparable to the driving rf wavelength. There are many system configurations for inductive sources. The planar coil configuration has been extensively studied in recent years [1–9]. Beale *et al* measured argon emission intensity profiles using spatially-resolved optical emission spectroscopy [10]. They found that the emission intensity peaked in a ring-shaped region at one end of the cylinder adjacent to the location of the antenna, where the rf field is strongest. Mahoney *et al* [11] studied, experimentally, the electron energy distribution functions using rf-filtered Langmuir probes. They found that the average electron energy varies by 1–2 eV spatially, with the highest values of average energy occurring near those regions of strongest rf electric field. Vahedi *et al* [12] proposed an analytical model to describe the plasma heating mechanism in planar sources, which is valid for all collisionality regimes. They then used a diffusion model to determine the plasma density profile and the electron temperature in terms of the gas pressure and the source geometry. The effect of the reactor geometry on plasma uniformity was examined by Stittsworth and Wendt [13]. Their study showed a tendency for the radial location of the plasma density maximum to shift from the centre outward as the chamber height is decreased and pressure is increased.

These studies suggest that the plasma in an inductively coupled plasma discharge, especially a large size 13.56 MHz plasma source, is inherently non-uniform, and that the density distribution depends strongly on the manner in which the power is delivered to the system and on the electrical and geometric configurations of the system.

As a plasma source becomes larger, high uniformity becomes even more difficult to achieve [14, 15], due to the standing-wave effect. Treating the antenna coil as a transmission line system, a standing wave is formed by two waves with the same frequency travelling in opposite directions. This can cause the power dissipation along the antenna to be highly non-uniform. Because flat panel processing requires a deposition non-uniformity $\leqslant$5% over large substrate areas for each film [16], the standing-wave effect in a conventionally driven planar coil system for such an application will be intolerable.

To understand and control standing-wave effects, we developed a processing system with a planar coil embedded in the plasma [17]. The coil is driven through a tuning network that can change the standing wave ratio (SWR) as desired, independent of the matching network which is used to match the rf power supply to the coil system. In section 2, we describe the system and experimental apparatus for this large-area plasma source (LAPS). In section 3 we discuss theoretically and experimentally the way by which standing-wave effects can be controlled and a travelling wave can be launched. In section 4 we gives the experimental results and compare these to a volume-averaged (global) model. The concept and experimental procedure introduced in this study may be applied to any inductively coupled, large-area plasma source to control standing-wave effects and improve the plasma uniformity.

2. Plasma system and experimental apparatus

2.1. Plasma reactor

The plasma chamber is a rectangular stainless-steel box (71.1 cm $\times$ 61.0 cm $\times$ 20.3 cm) pierced horizontally (see figure 1) by a planar line array of eight quartz tubes (25.8 mm outside diameter, 22 mm inside diameter, and 80 cm in length) whose centrelines are 7.65 cm apart. The interiors of the tubes are at atmospheric pressure and are forced-air cooled. The rf-excited coil system consists of eight, 6.35 mm outside diameter copper tubes threaded through the interiors of the quartz tubes and connected in a series (serpentine) path or in various other configurations. There are eight stainless-steel tubes mounted vertically in the chamber, serving as gas feed lines. There are pinholes evenly spaced on each of the tubes to provide a uniform plane of gas feeding. The tuning and matching network is enclosed in a copper box on the side of the chamber. There are 25 viewing ports to provide for electrical or optical diagnostics. Both 300 mm diameter silicon wafers and 360 mm $\times$ 465 mm glass substrates can be mounted on the back side of the chamber door, which can be water cooled. When the door is closed, the substrate faces the antenna plane at a distance of 9 cm from the centre of the antenna plane array.

To control the standing-wave effects we designed a tuning network, which resides between the matching network and the exciting antenna. This tuning network can generate an exciting wave with any SWR, so that the standing-wave effects on the plasma density profile can be examined thoroughly and systematically. Figure 2 shows the schematic diagram of the electrical configuration. A three-terminal

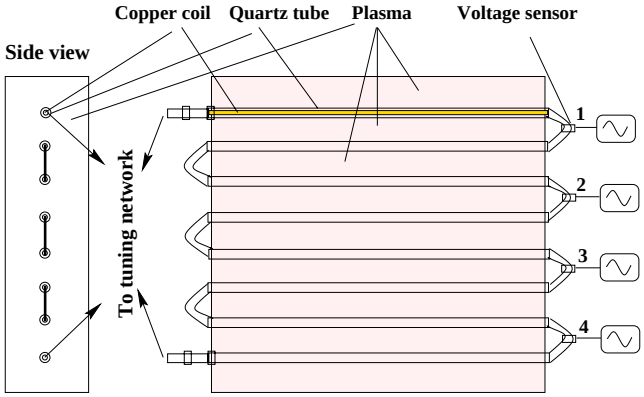

Figure 1. Antenna coil system. The coil is made of a series of copper tubes, each surrounded by a quartz tube embedded in the plasma. Four voltage sensors are equally spaced along the antenna coil to monitor the voltage distribution.

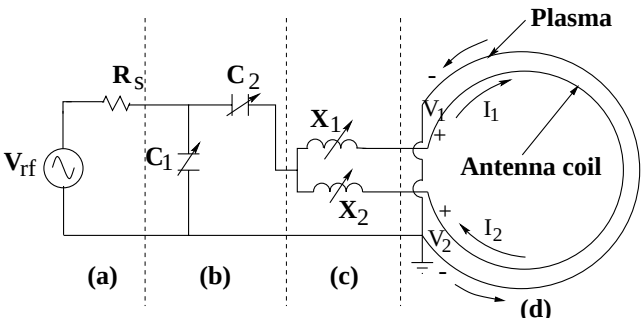

Figure 2. Schematic diagram of the circuit of the large-area plasma source system, with the tuning network shown to eliminate the standing-wave effect. $X_1 = \omega L_1$ and $X_2 = \omega L_2$ are two identical variable reactances with an adjustable range from 215 nH to 14 μH. (a), rf power generator; (b), matching network; (c), tuning network; and (d), antenna coil. In the actual tuning network used experimentally, X_1 and X_2 are each a parallel combination of a fixed inductor and a variable vacuum capacitor.

tuning network (c), consisting of two variable inductors, is used to control the SWR on the antenna coil (d). Each end of the antenna is connected to one of the inductors, and the other ends of both inductors are driven by the output of a two-port matching network (b) of the usual design appropriate to an inductive antenna. The input of the matching network is driven by a 13.56 MHz rf power supply (Advanced Energy Model RFX2500) (a). The power supply provides an adjustable output power from 0 to 2500 W.

2.2. Langmuir probe and data acquisition system

The measurements of the plasma densities under various operating conditions are made with Langmuir probes. The variation of the ion saturation current with voltage is used to calculate the plasma densities, based on the orbital ion motion model for cylindrical Langmuir probes [18, 19].

The probe consists of a tungsten wire sealed into a series of ceramic tubes. The probe tip, which is in contact with the plasma, is a tungsten wire 0.05 mm in diameter and 2 mm in length. The probe is mounted on a vertical rod inside the processing chamber and is driven by a stepping motor controlled by a computer through a data acquisition (DAQ) board. The DAQ board is also used to obtain plasma characteristic curves for further processing.

2.3. Travelling wave monitoring system

The antenna SWR is characterized using four voltage sensors equally spaced along the antenna coil as shown in figure 1. The voltage sensors are 1 cm wide, 2.54 cm diameter copper cylinders mounted concentrically with the antenna rods which capacitively couple the antenna coil voltage to the measuring circuit. The signals picked up by the voltage sensors are immediately converted into dc signals by four HP M12DM RF probes. Since the rf wavelength in our system is 11–15 m, depending on the plasma conditions, and since the total length of the transmission line of our system is about 8.5 m, four voltage sensors are enough to reveal the SWR. To facilitate the real-time tuning network and matching network adjustments, the four spatially-separated dc signals are displayed in one time-multiplexed oscilloscope channel.

3. Transmission line model

A transformer model is used to relate plasma parameters and system geometric configurations to circuit elements in a model transmission line. The model is used to determine the plasma properties experimentally through the measurement of the electrical properties of the system and provide the information necessary for the design of the matching and tuning networks.

In an inductively coupled system, the antenna acts as a primary coil and the plasma acts as a lossy secondary coil in a transformer [20]. The power is coupled from the primary to the secondary by transformer action. Since the physical length of the antenna in our system is comparable to the rf wavelength, unlike most reported systems where the antenna–plasma system is modelled using lumped circuit elements, we use a coaxial transmission line model, with the antenna (copper tubes inside the quartz tubes) comprising the inner conductor and the plasma surrounding the quartz tubes comprising the lossy outer conductor (see figure 3(a)). In this figure, the primary winding of the transformer represents the exciting antenna coil with inductance per unit length L_{11}. The one-turn secondary winding represents the plasma, with inductance per unit length $L_{22} + L_e$ and resistance per unit length R_p, where L_{22} is the geometric inductance that is determined by the discharge current path in the plasma, and L_e is the electron inertia inductance [21]. The elements in the secondary winding can be transformed to the primary winding where they combine with the elements in the primary winding to form the input impedance as seen by outside circuit, as shown in figure 3(b). This is done through the inductance matrix for an ideal transformer [22],

$$V_{rf} = \mathrm{j}\omega L_{11} I_{rf} + \mathrm{j}\omega L_{12} I_p \tag{1}$$

$$V_p = \mathrm{j}\omega L_{21} I_{rf} + \mathrm{j}\omega L_{22} I_p \tag{2}$$

with $V_p = -I_p(R_p + \mathrm{j}\omega L_e)$, referring to the circuit shown in the figure 3(b). The input impedance per unit length, or the impedance at the coil terminal is then defined as

$$Z_s = R_s + \mathrm{j}\omega L_s = \frac{V_{rf}}{I_{rf}} = \mathrm{j}\omega L_{11} + \frac{\omega^2 L_{12}^2}{R_p + \mathrm{j}\omega(L_p + L_e)}. \tag{3}$$

Clearly, L_{22}, L_e, and R_p are dependent on the plasma properties, such as discharge geometry, density, and temperature. Therefore, the values of these circuit elements can only be evaluated for a specified system configuration and plasma condition. Figure 4 shows the detailed structure and geometry of the antenna coil (primary winding) and its coupling to the plasma (secondary winding). Two neighbouring sections of the transmission line are shown. Applying the transformer model to this system, its equivalent circuit is shown in figure 3(a). Since the current induced in the plasma decays exponentially with the distance away from the quartz tube wall, the current in the plasma can be treated as confined in a thin layer outside the quartz tube, having a skin depth $\delta \equiv \alpha_p^{-1}$ as shown in figure 4, where α_p is the spatial decay constant. The spatial decay constant for the plasma can be estimated as [20]

$$\alpha_p = \frac{\omega}{c}\mathrm{Im}\,(\kappa_p^{1/2})$$

where the relative plasma dielectric constant κ_p is

$$\kappa_p = 1 - \frac{\omega_{pe}^2}{\omega(\omega - \mathrm{j}\nu_{eff})} \tag{4}$$

where ν_{eff} is the effective electron–neutral collision frequency and ω_{pe} is the electron plasma frequency [23].

In figure 3(b), the transformer for a unit length is redrawn to resemble a conventional transformer diagram. The inductances, capacitance, and resistance per unit length, L_{11}, L_{12}, L_{21}, L_{22}, L_e, C, and R_p are evaluated referring to the geometric diagram in figure 4 as

$$L_{11} = \frac{\mu_0}{2\pi}\ln\frac{d-a}{a}$$

$$L_{12} = L_{21} = \frac{\mu_0}{2\pi}\ln\frac{d-a}{b+\delta}$$

$$L_{22} = L_p = \frac{\mu_0}{2\pi}\ln\frac{d-b-\delta}{b+\delta}$$

$$C = \frac{C_a C_q}{C_a + C_q} \tag{5}$$

$$L_e = \frac{R_p}{\nu_{eff}}$$

$$R_p = \frac{1}{\sigma_{eff}}\frac{1}{\pi[(\delta+b)^2 - b^2]} \tag{6}$$

where, as shown in figure 4, a is the outer radius of the copper tube, b is the outer radius of the quartz tube, δ is the plasma skin depth, d is the centre distance between two neighbouring copper tubes, σ_{eff} is the effective plasma conductivity which may be expressed as

$$\sigma_{eff} = \frac{e^2 n_s}{m\nu_{eff}}$$

and C_a and C_q are the capacitances per unit length of the air gap and quartz, respectively:

$$C_a = \frac{2\pi\epsilon_0}{\ln((b-t)/a)} \tag{7}$$

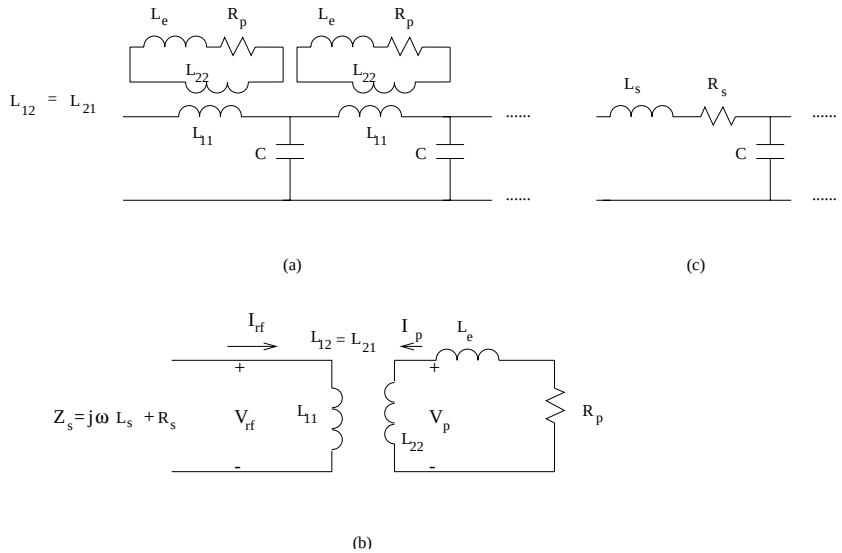

Figure 3. Equivalent circuit of the transmission line, showing transformer coupled plasma system: (a) coupled coil–plasma system, (b) transformer model and (c) equivalent transmission line.

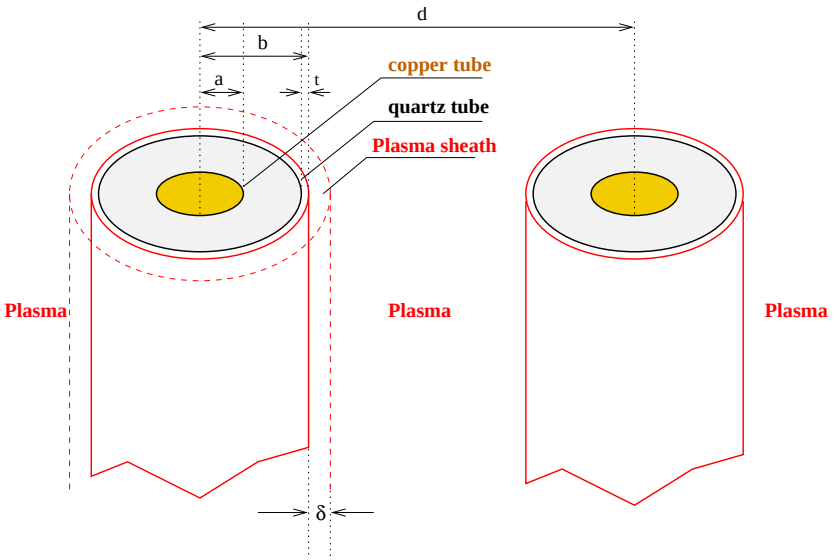

Figure 4. The structure and geometry of the coil–plasma transmission line model: a is the outer radius of the copper tube, b is the outer radius of quartz tube, d is the centre distance between two neighbouring copper tubes, δ is the plasma skin depth, and t is the quartz tube thickness.

$$C_q = \frac{2\pi\epsilon_0\epsilon_r}{\ln(b/(b-t))} \tag{8}$$

where t is the quartz tube thickness. C is the capacitance per unit length of the parallel combination of the air gap and quartz. The resistance per unit length R_p accounts for the power dissipation in the plasma, and the inductance per unit length L_e accounts for the additional energy storage in the plasma due to the electron inertia. The transmission line shown in figure 3(a) may be reduced to that shown in figure 3(c) with the corresponding transmission line parameters given by equation (3).

The characteristic impedance and wave propagation constant of the transmission line is then evaluated as [24]

$$Z_0 = \sqrt{\frac{\mathrm{j}\omega L_s + R_s}{\mathrm{j}\omega C}} \equiv R_0 + \mathrm{j}X_0 \tag{9}$$

and

$$\gamma = \sqrt{(\mathrm{j}\omega L_s + R_s)(\mathrm{j}\omega C)} \equiv \alpha + \mathrm{j}\beta \tag{10}$$

respectively. Both Z_0 and γ, like R_s and L_s, are dependent on the plasma conditions. A typical plasma environment for an inductively coupled system may be specified by choosing a typical plasma density at the plasma-sheath edge $n_s = 10^{11}$ cm^{-3} and a typical electron temperature $T_e = 3$ V. We also choose the following parameters according to our system configuration: $a = 0.635$ cm, $b = 1.27$ cm, $f = 13.56$ MHz, $p = 5$ mTorr. For these choices, we find $n_g = 1.7 \times 10^{14}$ cm^{-3}, $\nu_m = 1.4 \times 10^7$ s^{-1}, $\nu_{stoc} = 1.1 \times 10^7$ s^{-1}, $\sigma_{eff} = 112.5\ \Omega^{-1}$ m^{-1}, and $\delta = 1.68$ cm, where p is the gas pressure and n_g is the gas density. Using the above equations, we then find that $C = 80.2$ pF m^{-1}, $L_s = 0.365\ \mu$H m^{-1}, $R_s = 1.81\ \Omega$ m^{-1}, $Z_0 = (67.51 - \mathrm{j}1.965)\ \Omega$, $\alpha = 0.0134$ m^{-1}, and $\beta = 0.47$ m^{-1}.

In order to control the standing-wave effect, we have to choose an appropriate way to excite the antenna. We use a lossless tuning network which resides between the matching network and the exciting antenna, as shown in figure 2. Since the characteristic impedance varies with plasma conditions, the tuning network must be able to tune properly under different operating conditions. Two variable inductors are used in this design. In the practical implementation used for the experiments, parallel combinations of a fixed inductor and a variable capacitor are used. In the following, transmission line theory is used to derive the conditions required for the tuning network to control the antenna SWR and to launch a travelling wave.

The antenna and tuning network are shown in figure 5 with appropriate coordinates. The wave equations for a transmission line can be written as

$$\frac{\partial^2 V(z)}{\partial z^2} + \gamma^2 V(z) = 0$$

$$\frac{\partial^2 I(z)}{\partial z^2} + \gamma^2 I(z) = 0.$$

The solutions are

$$V = V_+ \mathrm{e}^{-\gamma z} + \rho V_+ \mathrm{e}^{\gamma z} \tag{11}$$

$$I = Y_0(V_+ \mathrm{e}^{-\gamma z} - \rho V_+ \mathrm{e}^{\gamma z}) \tag{12}$$

where $Y_0 \equiv G_0 + \mathrm{j}B_0 = Z_0^{-1}$ is the characteristic admittance, and $\rho = V_-/V_+$ is the complex reflection coefficient, which may be expressed as $\rho = \rho_r + \mathrm{j}\rho_i$, where ρ_r and ρ_i are the real and imaginary parts of ρ, respectively. Evaluating equations (11) and (12) at $z = \pm d$, we obtain

$$V(\pm d) = V_+ \mathrm{e}^{\mp(\alpha+\mathrm{j}\beta)d} + \rho V_+ \mathrm{e}^{\pm(\alpha+\mathrm{j}\beta)d} = V_{2,1} \tag{13}$$

$$I(\pm d) = Y_0(V_+ \mathrm{e}^{\mp(\alpha+\mathrm{j}\beta)d} - \rho V_+ \mathrm{e}^{\pm(\alpha+\mathrm{j}\beta)d}) = I_{2,1} \tag{14}$$

where l is the antenna length and $d = l/2$. Applying Kirchhoff's law, we have

$$V_2 = \mathrm{j}X_1 I_1 + V_1 + \mathrm{j}X_2 I_2 \tag{15}$$

For any given values of V_+ and ρ, the complex linear system (13)–(15) can be solved to obtain

$$\begin{aligned} X_{1,2} = D^{-1}\{&[2\rho_i B_0 + G_0(\rho_r^2 + \rho_i^2 - 1)]\cos\beta l \\ &\mp B_0[(\rho_r - 1)^2 + \rho_i^2]\sin\beta l + [G_0(1-\rho_r) - \rho_i B_0]\,\mathrm{e}^{\mp\alpha l} \\ &-[G_0(\rho_r^2 + \rho_i^2) + \rho_i B_0 - \rho_r G_0]\,\mathrm{e}^{\pm\alpha l}\} \end{aligned} \tag{16}$$

where

$$D = (B_0^2 + G_0^2)[\rho_i(\mathrm{e}^{-\alpha l} - \mathrm{e}^{\alpha l}) + (\rho_r^2 + \rho_i^2 - 1)\sin\beta l] \tag{17}$$

along with the complex variables V_1, V_2, I_1, and I_2. Equation (16) shows that for a given pair of ρ_r and ρ_i, there are always a pair X_1 and X_2 such that the relation expressed by (16) is satisfied. This means that by adjusting the values of X_1 and X_2, a wave with any desired SWR can be launched. The required values of tuning elements for launching a travelling wave are evaluated by setting $\rho = \rho_r + \mathrm{j}\rho_i \equiv 0$ in equations (16) and (17), to obtain

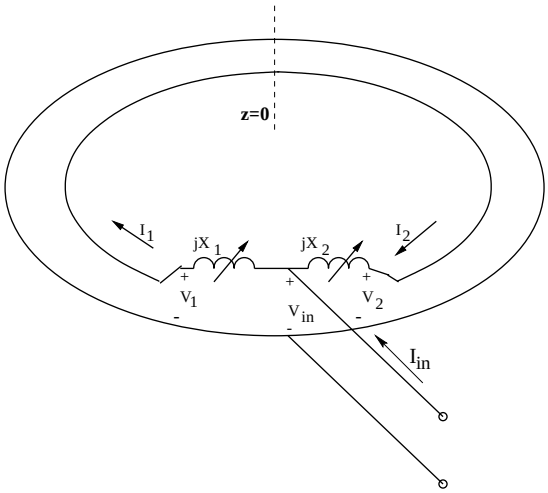

Figure 5. Schematic diagram of the circuit used to derive the tuning conditions, showing a looped transmission line. X_1 and X_2 are the reactances of the tuning elements. The total length of the transmission line is l and the distance from $Z = 0$ to the terminal point is $d = l/2$.

$$X_{1,2} = \frac{-G_0 \mathrm{e}^{\mp\gamma l} \pm (B_0 \sin\beta l \pm G_0 \cos\beta l)}{(B_0^2 + G_0^2)\sin\beta l}. \tag{18}$$

Equation (18) gives the required reactances of elements X_1 and X_2 to achieve a pure travelling wave along the antenna coil. The reactances X_1 and X_2 against R_s, the transmission line resistance per unit length, are plotted in figure 6 for three different transmission line lengths chosen to correspond to the experimental model system described below. This figure illustrates that whenever a change in plasma conditions occurs, X_1 and X_2 must be adjusted accordingly to ensure a pure travelling wave on the transmission line. The figure also shows that under typical plasma operating conditions, i.e. $R_s = 1$–$3\ \Omega$, and for the desired length of transmission line in our system, $l \approx 8.5$–9.5 m, the tuning elements X_1 and X_2 remain inductive; hence, in practice, a tuning network with two variable inductors only is capable of appropriate adjustment. The fact that X_1 and X_2 are equal at $R_s = 0$, as shown in figure 6, indicates that if there is no power dissipation in the system, a pure travelling wave would be unachievable—due to the symmetry, the tuning system would not favour a wave travelling in one direction over another.

It is worthwhile to mention that since both the tuning network and the exciting coil are symmetric, the X_1 and X_2 are commutable, which means that the forward and backward travelling waves are arbitrary defined, and that the tuning network is capable of launching a pure forward or backward wave, or a wave with any SWR. This provides a feasible way to experimentally study the relation between SWR, system configuration, and plasma conditions.

An experimental model system was built to study the electrical properties of the transmission line, tuning, and matching network. The model system was an aluminium box with eight sections of RG 312/U coaxial cable of total length 8.9 m placed inside with characteristic capacitance $C = 101$ pF m^{-1} and impedance $Z_0 = 50\ \Omega$. The outer

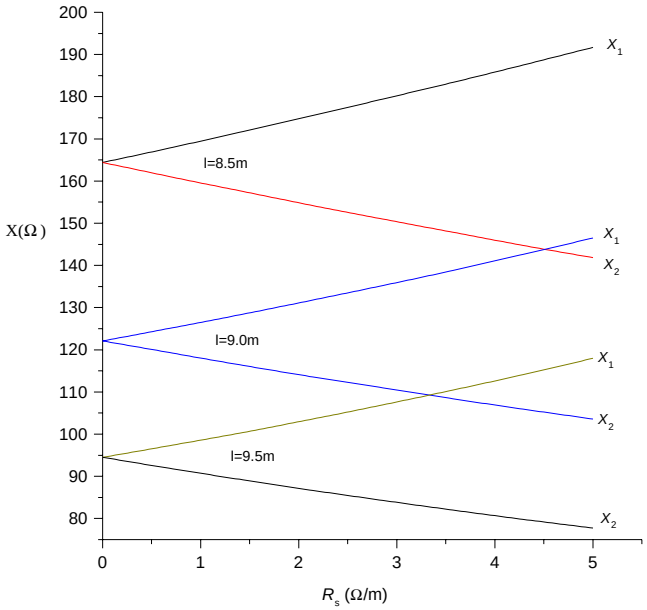

Figure 6. Reactances of the tuning elements against R_s with transmission line length l as a parameter. The cases for $l = 8.5$, 9.0, and 9.5 m are shown.

Table 1. Modelling system and plasma system comparison

Values for $f = 13.56$ MHz	Plasma system	Model system
C	80.2 pF m^{-1}	101 pF m^{-1}
L_s	0.365 μH m^{-1}	0.247 μH m^{-1}
R_s	1.81 Ω m^{-1}	1.80 Ω m^{-1}
Z_0	67.51 − j1.9651 Ω	50.40 − j1.9992 Ω
α	0.0134 m^{-1}	0.0168 m^{-1}
β	0.47 m^{-1}	0.426 m^{-1}

shields of the coaxial cables were broken, and a set of resistors was connected in series with the outer shields of each coaxial cable section. These resistors were varied to simulate different plasma loadings. Table 1 shows a comparison of transmission line parameters between the model system and the plasma system evaluated here for $p = 5$ mTorr and plasma $n = 10^{17}$ m^{-3}. The experimental model system has similar characteristics to those of the plasma system.

By adjusting the tuning element values X_1 and X_2 shown in figure 2, we observed the complete disappearance of the backward, or forward, travelling wave for the model system for various driving frequencies and coaxial shield resistances. The experimental results were in good agreement with the theoretical evaluation in equation (18). Further details are presented in [24].

4. Experimental results

4.1. Plasma density profiles

The plasma density profile can be influenced by the way in which the power is dissipated in the system. This can be changed by varying the exciting antenna configuration and standing-wave pattern along the antenna. Experiments were conducted for three different antenna configurations as shown in figure 7 and various SWRs. In figure 7(a), all eight sections

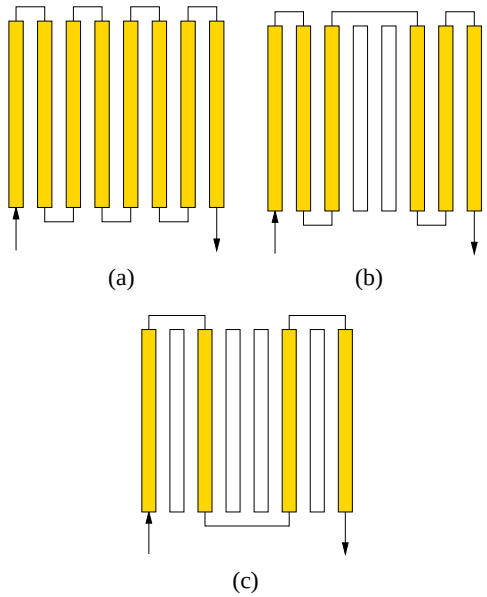

Figure 7. Schematic diagram of the different antennae configurations: (a) all rods are powered, (b) six rods are powered, and (c) four rods are powered.

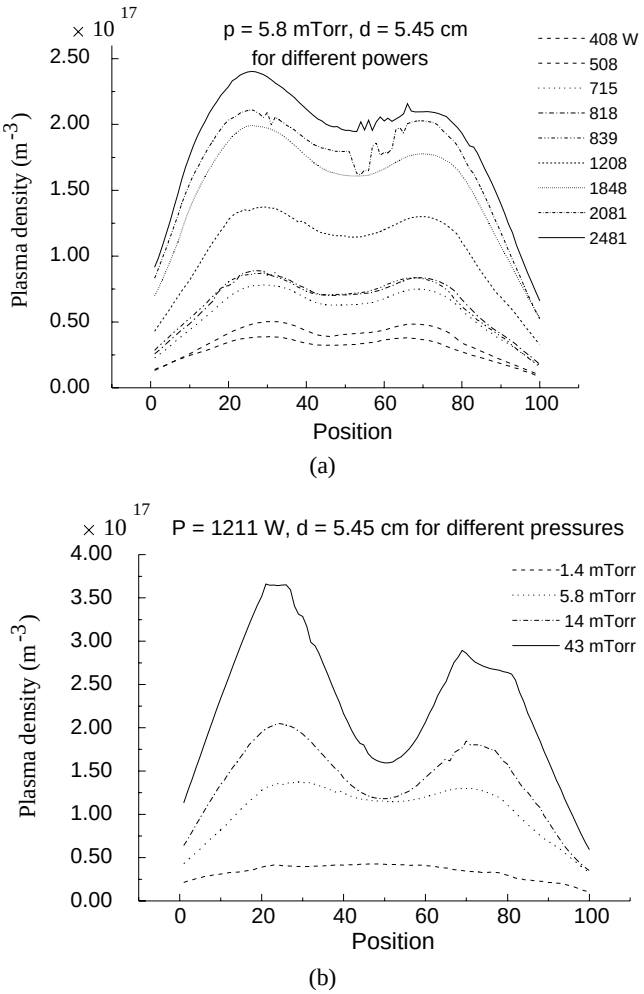

Figure 8. Plasma density profiles for (a) $p = 5.8$ mTorr, varying power, and (b) $P = 1211$ W, varying pressure. d is the distance between the antenna plane and the probe position.

of the antenna are powered; in figure 7(b), six of them are powered; and in figure 7(c), only four of them are powered.

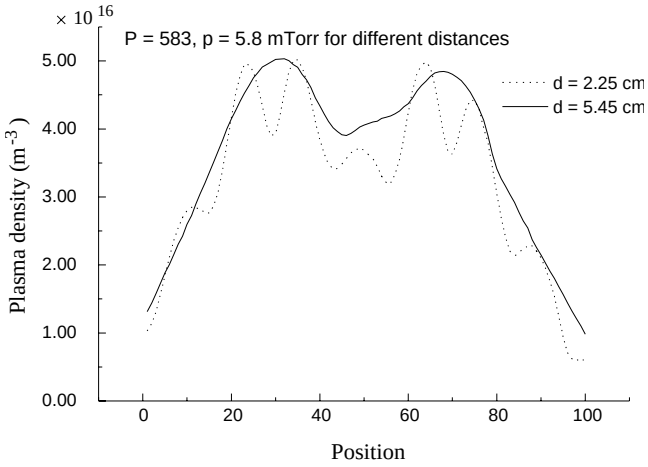

Figure 9. Plasma density profile for $d = 2.25$ and 5.45 cm, where d is the probe position with respect to the antenna plane.

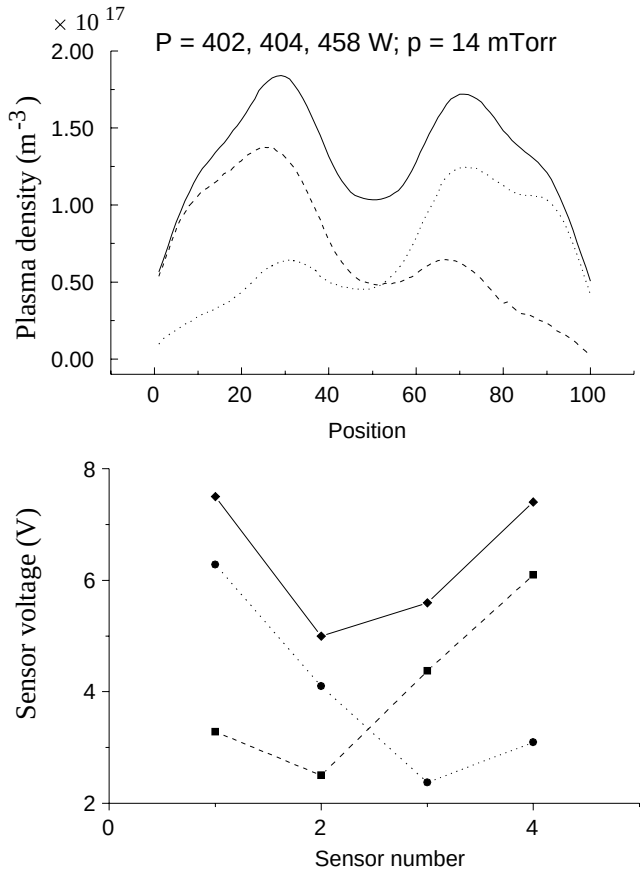

Figure 10. Plasma density profile and sensor voltage for $p = 14$ mTorr.

Both our theoretical analysis and experiments indicated that when all the eight rods are powered, the total transmission line length is about a half-wavelength of the rf driving power, depending on the plasma condition. This results in a resonance in the tuning network, causing a significant fraction of the input power to be dissipated in the tuning elements, and the discharge tends to be more capacitive. The experimental results under such circumstances will not reflect the true characteristics of the system, and we therefore do not present them in this discussion. For the experimental model system we did not operate near this resonance. There are a

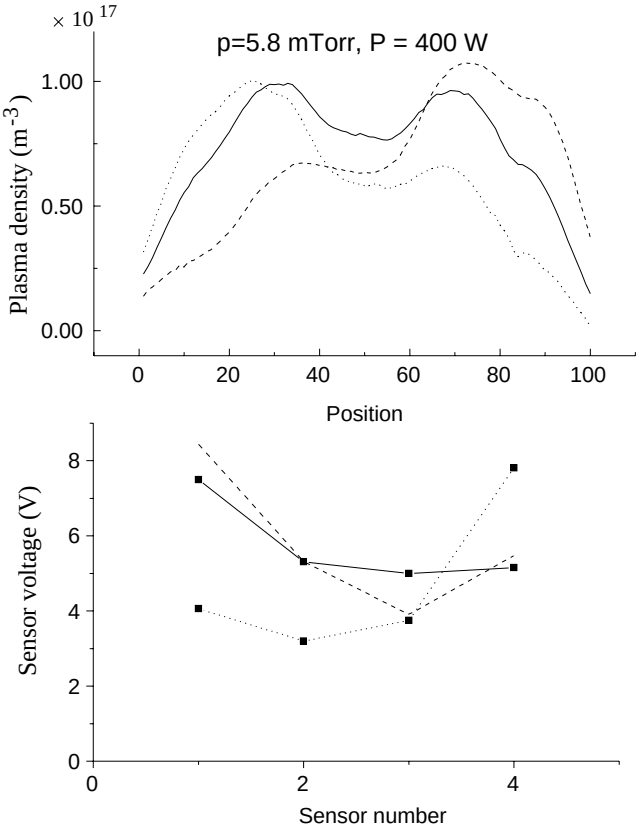

Figure 11. Plasma density profile and sensor voltage for $p = 5.8$ mTorr.

few approaches to eliminate the tuning network resonance. One of them is to change the antenna length, as we did for the configurations when six or four rods were powered, another is to modify the geometry of the antenna coil and hence the characteristic impedance. Detailed discussions about the tuning network resonance are beyond the scope of the current study and will be presented in another article.

4.1.1. Six rods powered. Figures 8 and 9 show the experimental results for the situation where six rods were powered. Figure 8(a) shows the density profiles for various input powers at an argon pressure $p = 5.8$ mTorr, while figure 8(b) shows the plasma density profiles for various gas pressures at an input power $P = 1211$ W. If all eight rods were powered uniformly, we would expect a sinusoidal density profile or something similar. With the middle two rods unpowered, we see from figure 8 that for pressures exceeding 1.4 mTorr, the density profiles have a minimum at the middle position. The experiments show that the antenna configuration can strongly influence the plasma density profile. Although in the experiments that generated the density profiles in figure 8 we kept the SWR to be essentially the same, the relative depth of the minimum of the profile increase with an increase in pressure. This suggests that for a fixed power, there exists a pressure at which the density profile is the flattest, as shown in figure 8.

For the data shown in figure 8, the system was tuned to optimize the uniformity of the density profile. This occurred at a finite SWR, with good matching conditions. The voltage distributions corresponding to the experimental results are

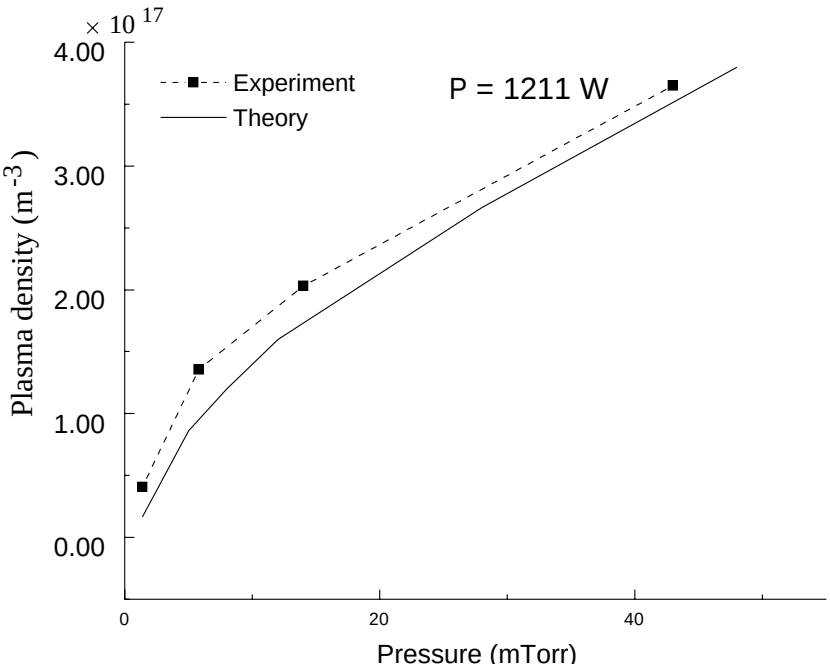

Figure 12. Plasma density against argon pressure showing the experimental results as compared with those from the global model for $P = 1211$ W.

symmetric about the centre line and the voltage values for the centre rods except the two unpowered rods are lower than those for the side rods. Our theoretical evaluation and experiments show that the voltage standing wave and current standing wave along the transmission line have a phase difference of π, which means that the current is high where the voltage is low. This means that the centre rods carried higher currents than the side rods. Since the power dissipation along the antenna is proportional to the square of the current, the plasma density is expected to be high where the voltage is low. As mentioned previously, a minimum in the density profile at the middle position is due to the two middle unpowered rods and the diffusive loss to the surfaces of the quartz rods. This minimum disappeared at low pressures, as shown in figure 8, when the diffusive loss to the walls of the middle rods is small. The fact that the density profiles shown in the figures are slightly deviated from the centre symmetry suggested by the voltage distributions may be due to the uncertainty in the voltage measurements, since the four voltage sensors cannot be exactly the same. There are glitches in the profiles at high power as shown in the figures. We believe that they are caused by either the probe breakdown or the disturbances resulted from the local sparks on the chamber walls. As expected, these phenomena are likely to occur at high powers. We also obtained good matches with pure travelling wave excitation, but density profiles were not as uniform as those shown in figure 8.

Figure 9 shows plasma density profiles for $d = 2.25$ and 5.45 cm, where d is the probe position with respect to the antenna plane. As expected, the density profile close to the antenna plane is embedded with the antenna pattern due to the diffusive loss of plasma to the surfaces of the quartz tubes. This suggests that for substrate processing, there should be an optimum distance between the substrate and the antenna plane at which the optimum uniform processing area can be achieved.

4.1.2. Four rods powered. To illustrate that the standing-wave pattern affects the plasma density profile and that the tuning network is capable of varying the density profile, experiments were performed to obtain plasma density profiles for different voltage distributions along the antenna. Figures 10 and 11 show the profiles with the corresponding voltage distributions along the antenna under conditions with a good match. As we can see, the density profile changes with the voltage distribution in a very predictable manner. The area with high voltage has a low plasma density and *vice versa*. As we mentioned previously, a high plasma density is expected where the voltage is low, and this is exactly the situation shown in figures 10 and 11. Since the voltage distribution along the antenna can be changed with the tuning network, this suggests that the plasma density profile in the processing chamber can be changed by appropriately adjusting the tuning network. From these experimental results, we see that the standing-wave pattern along the antenna can strongly vary the plasma density profile.

4.2. Plasma density compared with global model

A global model for inductive discharges can be used to predict the mid-position plasma densities under various operating conditions. In a global model, the species concentrations are spatially averaged [23]. It thus provides a simple physical picture and greatly reduces the computational resources required for modelling. It has been used by many researchers to analyse inductively coupled plasma sources [25–27]. The global model is based on the steady-state particle and energy balance equations, which state that the ionized particles generated in the plasma volume as well as the associated energy input must be equal to the particle and energy losses in the volume and through particle diffusion to the reactor walls. For given input power and gas pressure, the global model gives the average plasma density and temperature.

With the addition of a simple particle diffusion model, the density profile can also be approximated. For our inductive discharge, we make the simple approximation of a constant ambipolar diffusion coefficient D_a with a Bohm flux condition at the walls. This yields an electron temperature and a plasma density in the middle of the chamber that can be compared to experimental measurements. The diffusion solution is obtained using a finite-difference analysis performed in three dimensions for the chamber. To simplify the calculation, the round quartz tubes are replaced by tubes of square cross sections with the same surface area as the round tubes to account for plasma losses at the tube walls. We use an 'over-relaxation' iteration method [28] to solve the global model and diffusion equations to obtain the average plasma density, temperature and density profile.

Figure 12 shows the experimental results for the plasma density against the argon gas pressure as compared with the theoretical global model results. In comparing the experimental results with those from the global model, we must bear in mind that the global model assumes that the electron temperature is homogeneous and that the ionization occurs everywhere in the plasma at a rate proportional to the electron density. Hence the plasma density profile is independent of the power input into the system and the way in which it is delivered. In real situations, this may be true only for very low gas pressures. In the global model, the plasma density profile is determined by the geometry of the system only, while in practical situations, it is determined by the way the power is delivered in addition to the geometry. Therefore, we should not expect the experimental plasma density at a specific point in the system to agree with that from the global model. The trends of the increase in plasma density with pressure or power in experiments, however, should agree with those from the theory, if the power dissipation pattern remains the same during the course of pressure or power change; and in this sense, figure 12 shows an excellent agreement between the experiments and theoretical analyses.

5. Conclusions

In this study, we showed, for an inductively coupled plasma source with an antenna length comparable to the rf driving wavelength, that the exciting antenna configuration and standing-wave effect can strongly influence the plasma density distribution. The standing-wave effects can lead to a non-uniform plasma density, but can also be used to improve the density profile. The key is to launch a travelling wave or a wave with a desired SWR in a controllable manner. This was done in our study by using a simple lossless tuning network consisting of two variable reactive elements, either inductors or capacitors, depending on the driving antenna configuration. A travelling wave model was developed to determine the conditions for launching a wave with a given SWR, and this model was verified by experiments to be effective. We believe that this technique can be applied to any inductively coupled plasma source to improve the plasma uniformity when the driving antenna is a significant fraction of the driving rf wavelength. A global model was applied to our system configuration to evaluate the plasma density values and profiles, and the theoretical analysis was proved to agree well with the experiments.

Acknowledgments

This work was funded by National Science Foundation Grant ECS-9820836, California Industries, the Lam Research Corporation, and the State of California UC-SMART program under Contract 97-01. We gratefully acknowledge the assistance and suggestions of A J Lichtenberg.

References

[1] Singh V and Holland J 1996 *IEEE Trans. Plasma Sci.* **24** 133–4
[2] Hopwood J, Guarnieri C R, Whitehair S J and Cuomo J J 1993 *J. Vac. Sci. Technol.* **11** 152
[3] Hopwood J 1994 *Plasma Sources Sci. Technol.* **3** 460–4
[4] Stewart R A, Vitello P and Graves D B 1994 *J. Vac. Sci. Technol.* B **12** 478–85
[5] Gudmundsson J T and Lieberman M A 1998 *Plasma Sources Sci. Technol.* **7** 1–12
[6] El-Fayoumi I M and Jones I R 1997 *Plasma Sources Sci. Technol.* **6** 201–11
[7] Sobolewski M A 1997 *Phys. Rev.* E **56** 1001–11
[8] Samukawa S, Nakagawa Y, Tsukuda T, Ueyama H and Shinohara K 1995 *Appl. Phys. Lett.* **67** 1414–16
[9] Ventzek P L G, Hoekstra R J and J. K M 1994 *J. Vac. Sci. Technol.* **12** 461–77
[10] Beale D F, Wendt A E and Mahoney L J 1994 *J. Vac. Sci. Technol.* A **12** 2775–9
[11] Mahoney L J, Wendt A E, Barrios E, Richards C J and Shohet J L 1994 *J. Appl. Phys.* **76** 2041–7
[12] Vahedi V, Lieberman M A, Dipeso G, Rognlien T D and Hewett D 1995 *J. Appl. Phys.* **78** 1446–58
[13] Stittsworth J A and Wendt A E 1996 *Plasma Sources Sci. Technol.* **5** 429–35
[14] Wendt A E and Mahoney L J 1996 *Pure. Appl. Chem.* **68** 1055–8
[15] Munsat T, Hooke W M, Bozeman S P and Washbum S 1995 *Appl. Phys. Lett.* **66** 2180–2
[16] Crowley J L 1992 *Solid State Technol.* **35** 94–113
[17] Wu Y and Lieberman M A 1998 *Appl. Phys. Lett.* **72** 777–9
[18] Schott L 1968 *Plasma Diagnostics* (New York: North-Holland) ch 11, pp 669–95
[19] Wainman P N, Lieberman M A and Lichtenberg A J 1995 *J. Vac. Sci. Technol.* A **13** 2464–9
[20] Lieberman M A and Gottscho R A 1994 *Plasma Sources for Thin Film Deposition and Etching (Physics of Thin Films, vol 18)* ed M H Francombe and J L Vossen (New York: Academic) pp 1–119
[21] Piejak R B, Godyak V A and Alexandrovich B M 1992 *Plasma Sources Sci. Technol.* **1** 179–86
[22] Schwarz S E and Oldham W G 1984 *Electrical Engineering: An Introduction* (New York: Holt, Rinehard and Winston)
[23] Lieberman M A and Lichtenberg A J 1994 *Principles of Plasma Diagnostics and Materials Processing* (New York: Wiley)
[24] Wu Y and Lieberman M A 1995 Experimental modeling of a traveling wave-excited inductively driven coil for a large area plasma source *Memorandum* UCB/ERL M95/60 Electronics Research Laboratory, University of California, Berkeley
[25] Lee C and Graves D B 1994 *J. Electrochemical Soc.* **141** 1546–55
[26] Lee C and Lieberman M A 1994 *UCB/ERL* 49
[27] Ashida S and Lieberman M A 1997 *Japan. J. Appl. Phys.* **36** 854–61
[28] Booton R C J 1992 *Computational Methods for Electromagnetics and Microwaves* (New York: Wiley)

Annotations from 19026e.pdf

Page 5

Annotation 1
Equations OK as set.

Annotation 2
Changes OK here? or was `almost' meant?